Applied Surface Science 426 (2017) 391–398

Contents lists available at ScienceDirect

Applied Surface Science

journal homepage: www.elsevier.com/locate/apsusc

Full Length Article

Single-layer graphene/titanium oxide cubic nanorods array/FTO heterojunction for sensitive ultraviolet light detection☆

Feng-Xia Liang[a], Jiu-Zhen Wang[a], Yi Wang[b], Yi Lin[a], Lin Liang[a], Yang Gao[b], Lin-Bao Luo[b,*]

[a] School of Materials Science and Engineering, Hefei University of Technology, Hefei, 230009, China
[b] School of Electronic Science and Applied Physics, Hefei University of Technology, Hefei, 230009, China

ARTICLE INFO

Article history:
Received 21 April 2017
Received in revised form 13 June 2017
Accepted 5 July 2017
Available online 14 July 2017

Keywords:
UV light photodetector
Wide bandgap semiconductor
Light trapping effect
MSM junction
Responsivity

ABSTRACT

In this study, we report on the fabrication of a sensitive ultraviolet photodetector (UVPD) by simply transferring single-layer graphene (SLG) on rutile titanium oxide cubic nanorod (TiO_2NRs) array. The cubic TiO_2NRs array with strong light trapping effect was grown on fluorine-doped tin oxide (FTO) glass through a hydrothermal approach. The as-assembled UVPD was very sensitive to UV light illumination, but virtually blind to white light illumination. The responsivity and specific detectivity were estimated to be 52.1 A/W and 4.3×10^{12} Jones, respectively. What is more, in order to optimize device performance of UVPD, a wet-chemistry treatment was then employed to reduce the high concentration of defects in TiO_2NRs during hydrothermal growth. It was found that the UVPD after treatment showed obvious decrease in sensitivity, but the response speed (rise time: 80 ms, fall time: 160 ms) and specific detectivity were substantially increased. It is also found that the speicific detectivity was imporoved by six-fold to 3.2×10^{13} Jones, which was the best result in comparison with previously reported TiO_2 nanostructures or thin film based UVPDs. This totality of this study shows that the present SLG/TiO_2NR/FTO UVPD may find potential application in future optoelectronic devices and systems.

1. Introduction

Photodetectors, in particular ultraviolet photodetector (UVPD) working in UV light region, are receiving increasing research interest lately due to its potential application in a variety of fields including space communication, environmental monitoring, and military surveillance [1–4]. To date, a huge number of semiconductor materials with wide band gap such as III–VI group (e.g. GaN, AlN), II–VI group (e.g. ZnS and CdS), and some metal oxides (ZnO, SnO_2, and TiO_2) have been extensively investigated for fabrication of detectors for sensing UV illumination [5–8]. Among these wide-bandgap semiconductors, TiO_2 nanostructures in one-dimensional fashion (nanorods, nanotubes, nanosheets, *etc.*) are regarded as ideal candidates for realization of highly sensitive UVPD owing to their outstanding chemical, physical and optical properties [9–11]. To date, a number of UVPDs with good performance have been demonstrated. For example, Yang's group reported a double-walled carbon nanotube/TiO_2 nanotubes array heterojunction UVPD. By virtue of the dimensionality difference effect, the device exhibited a high photocurrent-to-darkcurrent ratio and photoresponse at a small bias voltage [12]. Recently, Wang et al. developed an UVPD by directly transferring different layers of TiO_2 nanorods (TiO_2NRs)-assembled cloth onto TiO_2NRs array [13], which was synthesized on conducting FTO coated glass. This devices showed outstanding UV selectivity with a response speed less than 0.3 s. In addition, the quantum efficiency of such an UVPD was as high as 46%. Despite these progresses, the majority of the TiO_2 nanodevices inevitably suffers from slow response speed, high darkcurrent, and poor reproducibility [14,15].

In order to optimize the device performance of TiO_2 based photodetectors, many groups have resorted to metal-semiconductor-metal (MSM) structures instead. Comparatively, the MSM device geometry is usually characterized by superior performance in term of high speed, low dark current and facile fabrication process [16]. What's more, the MSM structure can effectively suppress carrier recombination and enhance carrier transport [17], which is highly beneficial for a high on/off ratio during UV light sensing. Herein,

☆ This work was supported by the National Natural Science Foundation of China (NSFC, Nos. 21501038, 61575059, 61675062), the Fundamental Research Funds for the Central Universities (2013HGCH0012, 2014HGCH0005), and the China Postdoctoral Science Foundation (103471013).

* Corresponding author.
E-mail addresses: luolb@hfut.edu.cn, linbaoluo2@gmail.com (L.-B. Luo).

http://dx.doi.org/10.1016/j.apsusc.2017.07.051
0169-4332/

we report a new MSM UVPD by replacing metal with graphene, a very good electrode material with high electrical conductivity and transparency, and ultrahigh carrier mobility [18]. The combination of graphene and TiO_2NRs array with strong light trapping effect can simultaneously take advantage of the synergistic effects in photon harvesting and carrier transport, and thus it will greatly enhance the photosensitivity of the device. In order to reduce the defect concentration in the TiO_2NRs, we then adopted an effective wet-chemistry approach [19]. It was found that the SLG/TiO_2NRs/FTO UVPD device after treatment witnessed a great increase in on/off ratio, specific detectivity and response speed, even though the responsivity was reduced simultaneously. This study suggests that the present SLG/TiO_2NRs/FTO UVPD will have great potential for future optoelectronic device application.

2. Results and discussion

The scheme in Fig. 1(a) illustrates the step-wise procedure to fabricate the SLG/TiO_2NRs/FTO nanoheterojunction UVPD. The rutile cubic TiO_2NRs array was grown on FTO glass by a modified hydrothermal method [20]. After growth, a layer of graphene supported by polymethylmethacrylate (PMMA) was directly transferred onto the TiO_2NRs array by an aqueous method [21]. At last, Ag paste was placed directly onto the graphene and FTO side. For convenience, the as-fabricated nano-heterojunction was then assembled onto a printed circuit board (PCB). Fig. 1(c) shows a typical digital camera picture of the SLG/TiO_2NRs/FTO on a PCB, in which the two electrodes are connected to the PCB by wire bonding. Due to their apparent difference in contrast, all components including SLG, FTO and TiO_2NRs can be easily discriminated [Fig. 1(b)].

To check the quality of both materials, the morphology, crystallinity and chemical composition of both graphene and cubic TiO_2NR were examined. Fig. 2(a) shows the Raman analysis of the chemical vapor deposition (CVD) derived graphene, from which one can find two strong peaks: one at ~1511 cm^{-1} (G-band) and another at ~2633 cm^{-1} (2*D*-band). Additionally, there is also a very weak peak at 1346 cm^{-1}, which can be attributed to the *D*-band. The intensity ratio of 2.12 (I_{2D}/I_G) and the relatively weak *D*-band corroborates the single-layer feature with a little quantity of defects [22,23]. The Fig. 2(b) corresponds to scanning electron microscopy (SEM) image of the SLG at Si/SiO_2 wafer. Obviously, there are some wrinkles which were usually unavoidable during the transfer of graphene at water [24]. The representative top-view SEM image of the TiO_2NRs was shown in Fig. 2(c). It's clear that all the TiO_2NRs have a well-defined rectangular cross-section. The diameters were in the range from 50 to 140 nm, with an average value of about 100 nm [Fig. 2(d)]. According to the high-resolution transmission electron microscopy (HRTEM) image and the selected area electron diffraction (SAED) pattern shown in Fig. 2(e), the as-prepared TiO_2NRs were single crystalline of rutile phase, with a preferred growth orientation along the [001] direction [25].

Fig. 3(a) plots the *I–V* curve of the SLG/TiO_2NRs/FTO UVPD. Obviously, it displays a typical nonlinear behavior, as often in conventional MSM structure. Given the negligible contact barrier of both the Ag/SLG and Ag/FTO contacts (Fig. S1, Supporting Information), such a nonlinear *I–V* characteristics can be exclusively attributed to two Schottky junctions assembled in a back-to-back fashion [inset of Fig. 3(a)]: one is formed at FTO/TiO_2NRs interface, and the other one at the SLG/TiO_2NRs interface, which is different from other graphene-like 2D material-semiconductor heterojunction based devices [26,27]. Our optoelectronic analysis finds that this SLG/TiO_2NRs/FTO nanoheterojunction is virtually blind to white light illumination, but exhibits pronounced sensitivity once it was shined by UV illumination with wavelength of 365 nm [Fig. 3(b)], suggesting potential application for UV detection. Fig. 3(c) compares the photoresponse of three heterojunctions assembled from cubic TiO_2NR with different diameters. It is apparent that when the TiO_2NR diameter gradually increases from 100 to 180 nm, the photocurrent on the contrary decreases from 3.83 to 2.65, and 0.78 mA at a bias voltage of −5 V. This relatively high photoresponse for 100 nm TiO_2NR device is associated with the better light absorption capability, as we will discuss later. Further study found that the photoresponse of the UVPD is determined by the UV light intensity as well. Fig. 3(d) shows the *I–V* curves of the device under UV light radiation with varied intensities, from which one can observe that the photocurrent increases gradually with the increase of the UV intensity.

Besides diameter of TiO_2NR and wavelength of incident light, the photoresponse of the present nanoheterojunction UVPD is also found to be determined by bias voltage. Fig. 3(e) plots the photoresponse of the device at different negative bias voltages. At all bias voltages, the UVPD device showed good UV photosensivity when the 365 nm light was alternately switched on and off. Moreover, with the increase of the bias voltage (absolute value), the photocurrent will increase monotonically, possibly due to the increase in drift velocity and suppression in recombination possibility [28,29]. This bias voltage dependent photocurrent is slightly different from the case at forward bias voltage, under which the present device similarly shows pronounced sensitivity to UV illumination. Nonetheless, the darkcurrent is relatively higher than that at negative bias voltage (Fig. S2). In light of this, negative bias voltage will be applied on the UVPD in the following optoelectronic characterization. As a matter of fact, the obvious photoresponse at negative bias voltage can be explained by the energy band diagram shown in Fig. 3(f). Due to the different Schottky barrier heights (SBH), the two back-to-back Schottky junction was asymmetric, with a relatively larger built-in electric field at SLG/TiO_2NRs interface than that at FTO/TiO_2NRs. When applied by a negative bias voltage (the graphene side is negatively biased and the FTO side is positively biased), the SBH at SLG/TiO_2NRs interface will increase, while that of FTO/TiO_2NRs heterojunction will on the contrary decrease, as shown by red line. In this case, the electrons were difficult to flow from the TiO_2 side to the graphene in dark condition, leading to a low dark current. Upon UV light illumination, the photo-generated electron and holes could be separated by the electric field in opposite directions, forming photocurrent in the circuit.

In order to unveil the underlying reason for the aforementioned diameter dependent photosensitivity, the optical properties of TiO_2NRs array with different diameters under 365 nm UV illumination was then examined. Fig. 4(a–c) illustrate the distribution of electric field energy density distribution and the corresponding SEM of the TiO_2NRs with varied diameters. Obviously, the electric field distributions of TiO_2NRs array without SLG coverage (W/O) is almost identical to that of TiO_2NRs with SLG coverage (W/), consistent with the high transparency of single layer graphene [30]. Meanwhile, all the cubic TiO_2NRs display very good light trapping effect: That is, the incident photon energy will be efficiently confined within the nanostructures. The hot spot with high field intensity is about hundreds of nm below the SLG/TiO_2NRs interface, which is beneficial for the photosensing process. Such a light trapping effect is further confirmed by the simulated absorption spectrum of both TiO_2NRs array and its planar counterpart. As displayed in Fig. 4(d), in comparison with the cubic TiO_2NRs array, the planar TiO_2 shows relatively weak light absorption in the UV region due to the strong reflectance. Furthermore, among the three kinds of TiO_2NRs, the 100 nm TiO_2NR shows the highest light absorption than planar TiO_2 at around 365 nm, which is in good agreement with the previous result.

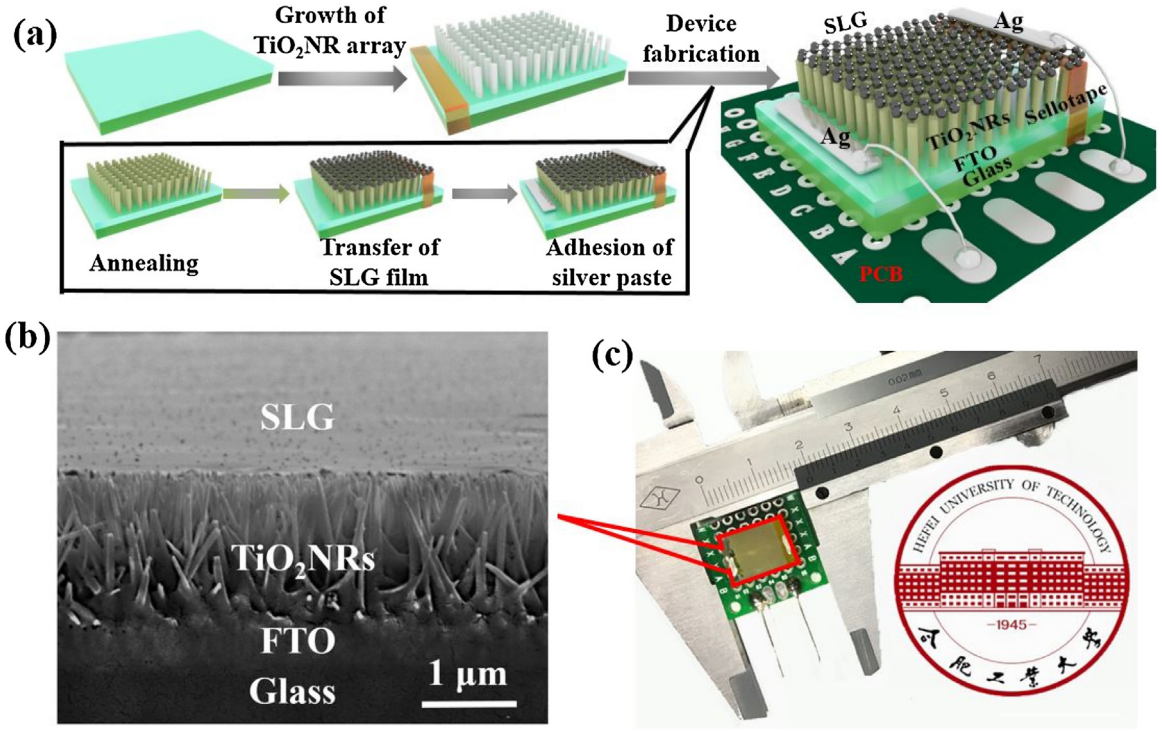

Fig. 1. (a) Schematic illustration of step-wise process for assembly of the SLG/TiO_2NRs/FTO nanoheterojunction UVPD. (b) Cross-sectional SEM image of the SLG/TiO_2NRs/FTO structure. (c) Digital camera picture of the UVPD device.

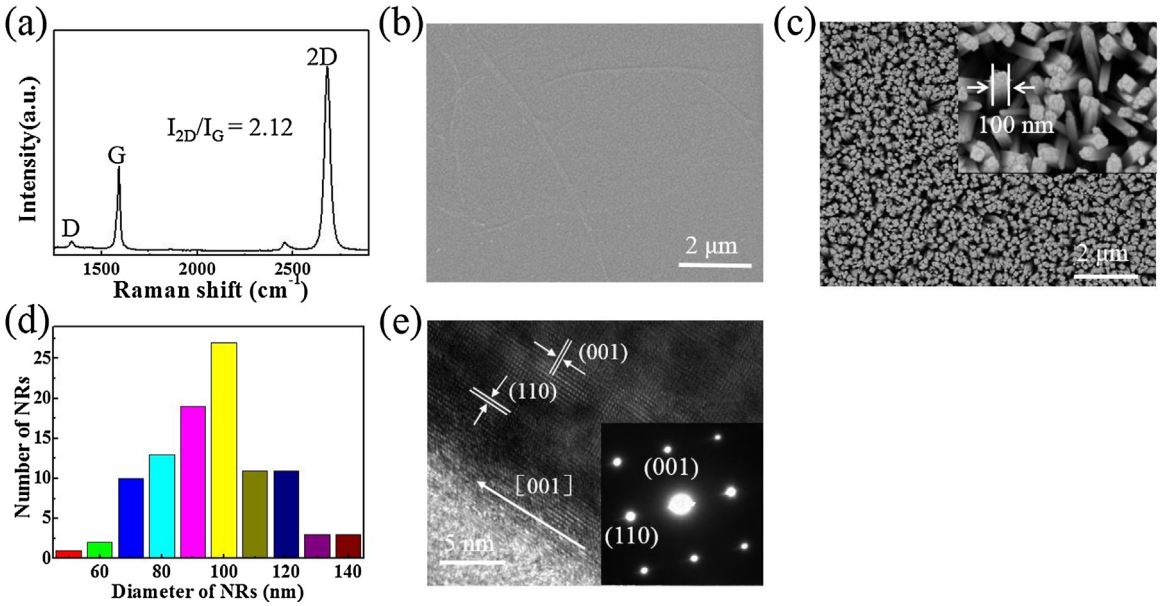

Fig. 2. (a) Raman analysis of the SLG film. (b) SEM image of the SLG film on a Si/SiO_2 wafer. (c) Top-view of the cubic TiO_2NRs array. (d) The diameter distribution of 100 TiO_2NRs. (e) HRTEM image, and the corresponding SAED pattern of a single cubic TiO_2NR.

Although the above result demonstrates that device performance of the present nanoheterojunction UVPD can benefit from the light trapping effect of cubic TiO_2NR array and the high transparence of the SLG. Unfortunately, this device has its own shortcoming in that there is always a huge amount of defects in the solution-processed TiO_2NR [31]. In order to optimize the device performance, we then adopted a wet-chemistry treatment to reduce the defect density usually in the form of oxygen vacancy (V_o) and Ti interstitials [32], which cannot be removed by conventional approaches. Fig. 5(a) compares the X-ray diffraction (XRD) patterns of FTO film, TiO_2NRs with and without treatment. It is shown that after treatment, all diffraction peaks due to rutile structure of TiO_2 (JCPDS: 21-1276) were considerably increased, indicative of great optimization in crystallinity. To shed light on the microstructural evolution during the treatment, both samples were then investigated by photoluminescence (PL) analysis shown in Fig. 5(b). The TiO_2NRs without treatment exhibits a broad emission in the wavelength from 550 to 900 nm. Additionly, there are three peaks centred at 575 nm (Peak 1), 650 nm (Peak 2) and 850 nm (Peak 3) (black curves). According to the previous study, [22,33,34]

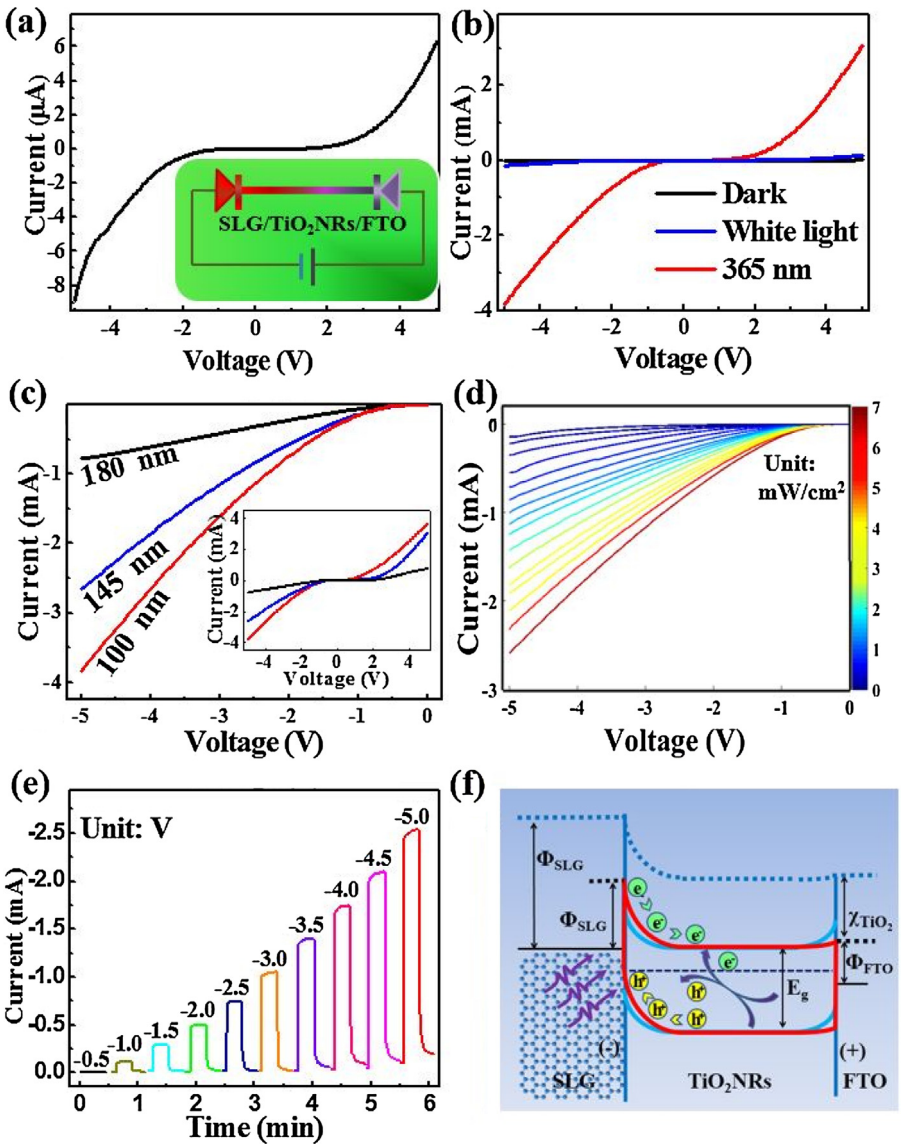

Fig. 3. (a) *I–V* characteristics of the UVPD in dark, the inset shows the device model composed of two back-to-back Schottky diode. (b) *I–V* characteristics of the device in dark, and under white light and 365 nm light illumination. (c) Photoresponse of the UVPDs assembled from different diameters of TiO_2NRs array at negative bias, the inset is the corresponding *I–V* curve in the bias range from −5 to 5 V. (d) The photoresponse of UVPD under various UV intensities. (e) The response of UVPD at negative bias voltages. (f) Energy band diagram of the SLG/TiO_2NRs/FTO UVPD at negative bias voltage.

the peak 1 and 2 can be ascribed to Ov-related trap state,while peak 3 correponds to Ti interstitials, in particular Ti_{int}^{4+}. Notably, the broad emission as well as peak 1 and 2 disappear all of sadden when the TiO_2NRs arrays was treated, implying that the majority of defects was sucessfully removed. In fact, this change in defects was further confirmed by X-ray photoelectron spectroscopy (XPS) analysis. Fig. 5(c) depicts the Ti2p spectra collected from both TiO_2NRs with and without treatment. Both spectra are composed of two obvious peaks due to the $2p_{1/2}$ and $2p_{3/2}$ states, respectively. In comparison to untreated sample, the binding energy of the TiO_2NRs after treatment shifts by 0.3 eV. This shift in binding energy is understandable as the presence of V_O and Ti interstitials in untreated TiO_2NRs can lead to an increment in electron density and thus a weaker binding effect [35–37]. By extrapolating the $(\alpha h\nu)^2$–hν plots in Fig. 5(d), the band gap (E_g) values for treated TiO_2NRs and untreated NRs are estimated to be about 3.02 and 2.97 eV, respectively. This slight change in bandgap is consistent with the spectral selectivity, which will be discussed later.

Like the untreated device shown in Fig. 3(d), the UVPD after chemical treatment also display excellent photoresponse to UV light illumination [Fig. 6(a)]. Fig. 6(b) shows the photoresponse of the UVPD as a function of light intensity. At all negtive bias voltages, the photocurrent is highly dependent on the intensity of the UV light. Specifically, the photocurrent at bias voltage of −5 V under the same UV illumination after treatment is only one fifth of that without treatment (Fig. S3). To quantitatively evaluate the effect of chemical treatment on the device performance, the responsivity that is defined by the photocurrent generated per unit power of the incident UV on the effective area of the device was calculated by using the following equation [38]:

$$R = \frac{I_\lambda - I_d}{P_\lambda A} \quad (1)$$

where, I_λ is the illumination current, I_d, P_λ, A the dark current, UV light intensity, and area of the UVPD, respectively. Based on these values, the responsivity of the UVPDs with and without treatment was calculated and summarized in Fig. 6(c). In the wavelength

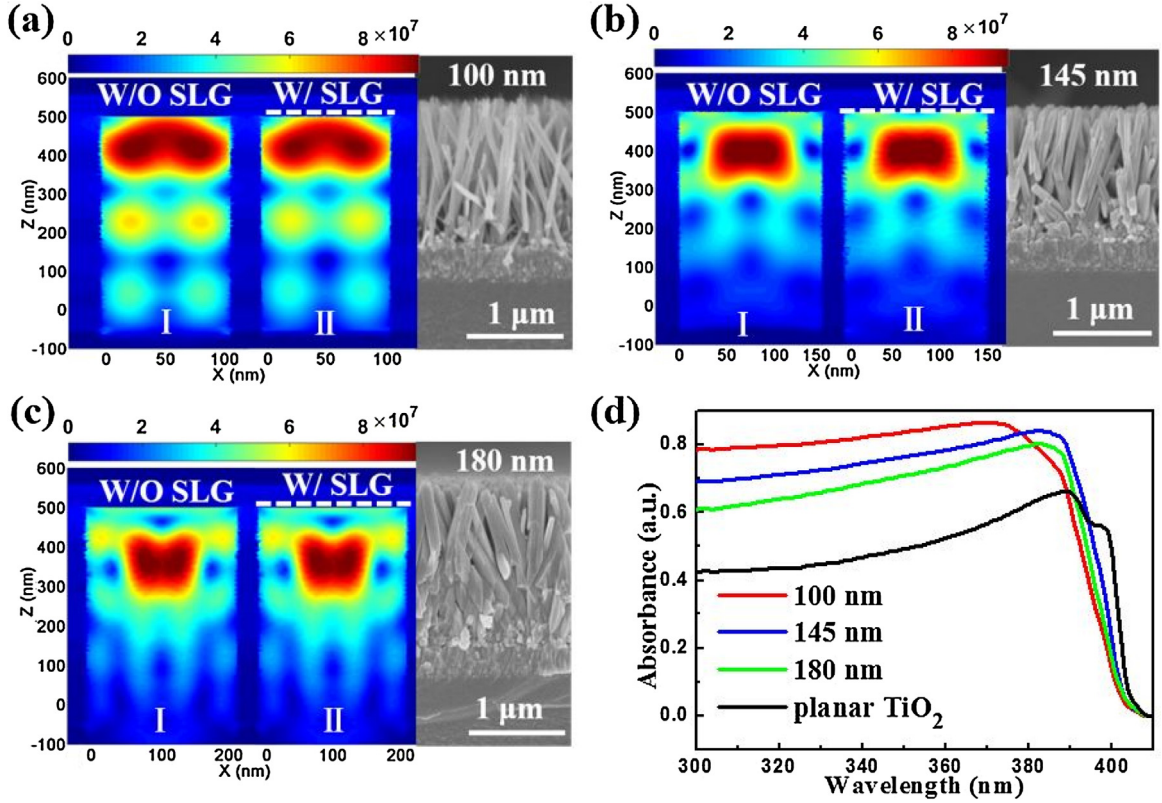

Fig. 4. Simulated electric field energy density distribution of the TiO_2NRs array with different diameters of 100 nm (a), 145 nm (b), 180 nm (c). (d) Theoretical absorption spectra of different types of TiO_2NRs.

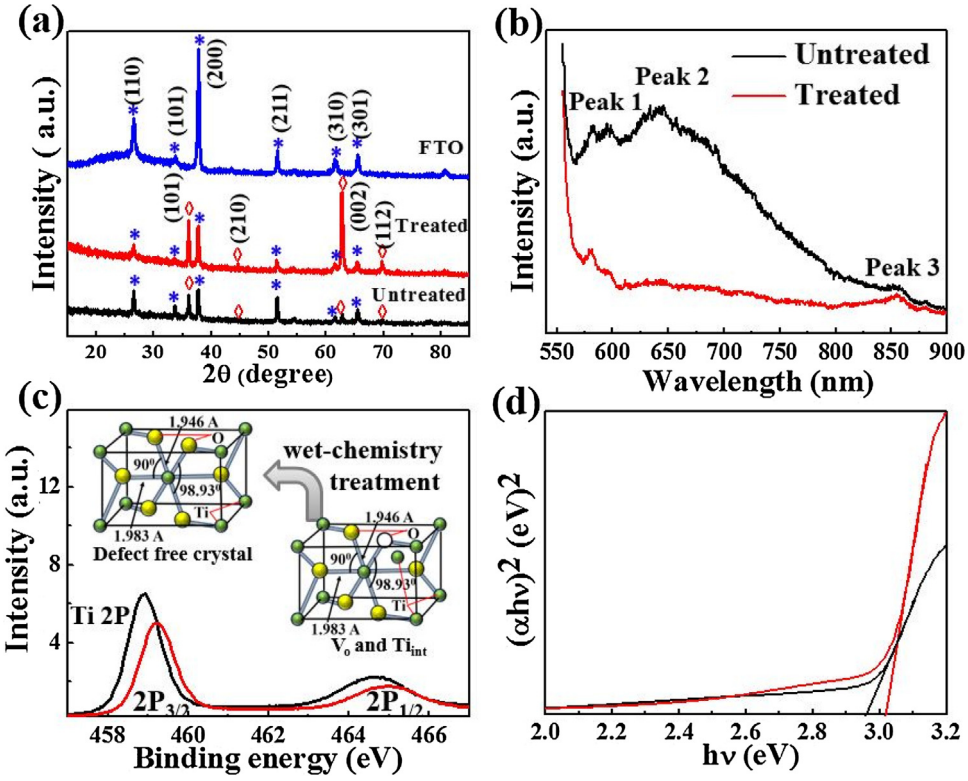

Fig. 5. (a) XRD patterns of FTO, untreated (black line) and treated (red line) NRs. (b) Photoluminescence (PL) spectra of TiO_2NRs (c) XPS spectra of the Ti $2P_{3/2}$ and Ti $2P_{1/2}$. (d) The plots of $(\alpha h\nu)^2$–$h\nu$ of TiO_2NRs array with and without treatment. (For interpretation of the references to colour in this figure legend, the reader is referred to the web version of this article.)

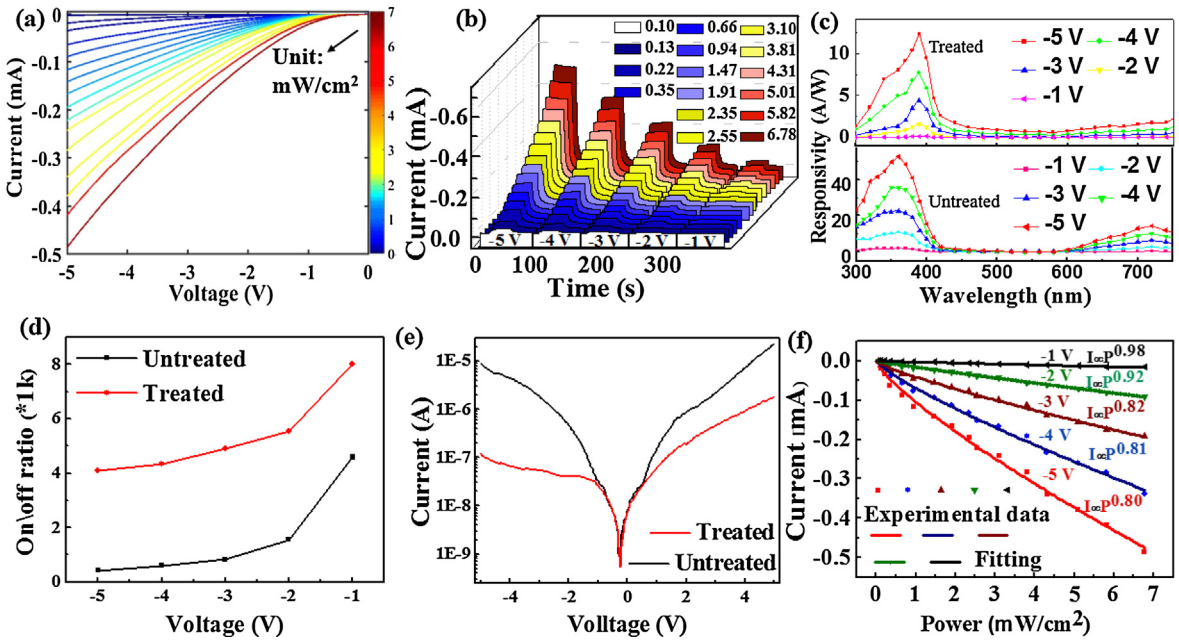

Fig. 6. (a) Photoresponse of the treated UVPD device under different light intensities at negative bias, λ = 385 nm, the color bar shows the UV intensity in unit of mW/cm^2. (b) Comparison of photocurrent of treated devices at different bias voltages. (c) The responsivity of the treated UVPD device at different bias voltages. (d) Comparison of on/off ratio of both treated and untreated devices. (e) Comparison of the dark current of both treated and untreated devices. (f) Photocurrent as a function of the light intensity at different bias voltages.

Table 1
Comparison of the device performance of the UVPD with and without treatment.

Device	Max D^*(Jones)	τ_r (ms)	τ_r (ms)	I_{light}/I_{dark}	Max R (A/W)
Untreated UVPD	4.3×10^{12}	1300	4600	414	52.1
Treated UVPD	3.2×10^{13}	80	160	4110	12.3

range from 300 to 750 nm. the maximum responsivity of the untreated UVPD is at least three times larger than that of treated device [39]. This decrease in responsivity is due to the reduced density of defects after the chemical treatment, which will lead to decrease in carrier concentration. As a result, both photocurrent and dark current were decreased. In spite of the adverse effect of chemical treatment to responsivity, it is however interesting to note that the on/off ratio will benefit from such treatment. Fig. 6(d) compares the on/off ratios of both devices with and without treatment. Apparently, the on/off ratio is found to increase dramatically after treatment. Further comparison of the darkcurrent reveals that this increase in on/off ratio directly stems from chemical treatment, which can directly reduce the defect level, and thereby reduce the electical conductivity of the TiO_2NR. As a matter of fact, such a reduce of defect density was also reflected by the relationship between the photocurrent and light intensity. Fig. 6(f) plots the photocurrent of the treated UVPD at different light intensities. The relationship between both phocurrent and light intensity can be described by a power law: $I = AC^{\theta}$ [40], where I, A, C and θ represent the photocurrent of UVPD, the constant for 365 nm, the incident UV intensity, and exponent determining the photoresponse of photocurrent to UV light, respectively. By using this formula, the θ is estimated to be 0.98, 0.92, 0.82, 0.81 and 0.80, for bias voltage of −1, −2, −3, −4 and −5 V, respectively. These values are much higher than that without treatment (Fig. S4). Understanably, this increase in exponent is owing to the reduce in defect density, considering the fact that the exponent is mainly determined by the defect density in the device [41].

Another beneficial effect of the treatment is the optimization in response speed, as summarized in Table 1. Fig. 7(a) compares the photoresponse of two SLG/TiO_2NRs/FTO UVPDs before and after

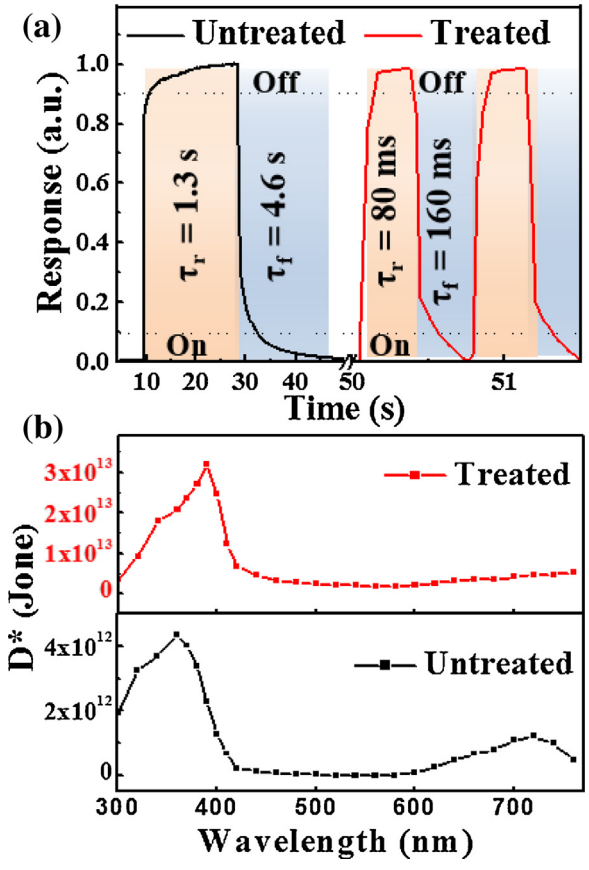

Fig. 7. Comparison of the response time (τ_r) and recovery time (τ_f) (a), and specific detectivity (b) of the UVPD devices with and without treatment.

treatment. The rise time and fall time for the treated device were estimated to be 80 and 160 ms, respectively, which are at least one order of magnitude faster than that without treatment (rise

time: 1.3 s, fall time:4.6 s). Finally, it is worth pointing out that the treatment can lead to optimized spectral selectivity and specific detectivity. The UVPD without treatment displays two peak sensitivity at both 365 and 710 nm. Nonetheless, the peak at longer wavelength will completely disappear, and the 365 nm peak sensitivity will change to 385 nm when the device was treated [Fig. 7(b)]. On the other hand, the maximum specific detectivity for the treated device at peak sensitivity is around 3.5×10^{13} Jones, which is nearly one order of magnitude higher than that of untreated device. Such an optimization due to the removal of defects including V_o and Ti interstitials is very interesting as it helps to open up new opportunities to optimize the device performance of other photodetectors.

3. Conclusion

In summary, we have fabricated a sensitive UVPD based on SLG/TiO_2NRs/FTO nanoheterojunction. The as-fabricated UVPD showed obvious sensitivity to 365 nm UV illumination. The device performance of this UVPD including on/off ratio and response speed can be considerably optimized by reducing the concentration of defects in the TiO_2NRs array using a simple chemical-treatment process. Furthermore, the specific detectivity of the device can be considerably increased from 4.3×10^{12} Jones to 3.2×10^{13} Jones, which is the best result when compared with other TiO_2 nanostructures or thin film based UVPDs. According to both experimental result and theoretical simulation based FEM, the high specific detectivity is related to not only the light trapping effect, but also due to the reduced defects concentration after treatment. The present high-performance UVPD is believed to have potential application in future nano-optoelectronic devices.

4. Experimental section

4.1. Materials synthesis

The TiO_2NRs array was synthesized by a hydrothermal method. Briefly, a commercial glass substrate with a layer of 100 nm fluorine-doped tin oxide was cleaned with acetone and distilled water to remove possible contaminants on the surface. Afterwards, the clean substrate was loaded into a 100 mL Teflon-lined stainless steel reactor, which was prefilled with 25 mL distilled water, 25 mL 37% HCl and 0.2 mL titanium tetrachloride. The reactor was then sealed and kept at 453 K for 2 h. After reaction, the glass substrate will be collected. In this study, the diameter of TiO_2NRs can be easily tailored by adjusting the ratio of H_2O and HCl. The graphene film was synthesized through a simple CVD approach that was performed in a tube furnace at a temperature of 1015 °C. In this growth process, 50 μm Cu foil and a mixed gas composed of CH_4 (1 SCCM) and H_2 (99 SCCM) will be used as catalytic substrate and reaction precursors, respectively. After synthesis, the graphene film will be transferred from the Cu foil by an aqueous method. Detailed description of this method can be found elsewhere [42]. The treatment was carried out by simply soaking TiO_2NRs array in H_2O_2–NH_3 (10:1) solution for 10 min, followed by 2 h annealing in oxygen atmosphere at 773 K.

4.2. Device assembly and analysis

The as-synthesized TiO_2NRs array was firstly struck with a layer of sellotape at four edges for insulation. The TiO_2NRs was then soaked into an aqueous solution with graphene film floating on the surface, and then lightly lifted to mount the SLG film the TiO_2NRs surface. Finally, silver paste was stuck onto the graphene, where the PMMA film was wiped off by acetone. The electrical property of the SLG/TiO_2NRs heterojunction was measured by using an *I–V* characterization system (Keithley 4200, SCS). What is more, for optoelectronic characteristics, the *I–V* characterization system will be combined with a monochromator (SP 2150, Princeton Co.), from which the UV light will be guided to the photodetector by optical fibers. Note that before all optoelectronic analysis, a powermeter (Thorlabs GmbH, PM100D) will be used to calibrate the power intensity of the incident UV light.

4.3. Theoretical simulation

In this simulation, we analyze the electric field intensity of TiO_2NRs array by using the COMSOL Multiphysics software, which is based on the finite element method in frequency domain images. We applied periodic boundary conditions applied in x and y direction to replicate our array structures. The perfectly matched layers have been used in propagation direction to absorb any reflected and transmitted fields. The incident light on top of the structure has a wavelength ranged from 300 to 400 nm. In addition, the permittivity of air is set to be 1. The permittivity of TiO_2NRs is obtained from the Filmetrics database. The conductivity of graphene can be described by a Drude-like expression: $\sigma_G = i\frac{e^2 k_B T}{\pi\hbar^2(\omega+i\tau^{-1})}\left\{\frac{E_f}{k_B T}+2\ln\left[\exp(-\frac{E_f}{k_B T})+1\right]\right\}$

where ω is the light angular frequency, T is the temperature, e is the electron charge, $\hbar$ is the reduced Planck's constant, k_B is the Boltzmann constant, E_f and τ are the chemistry potential and the momentum relaxation time, respectively (T = 300 K, E_f = 0.12 eV and τ = 0.5 ps). The permittivity of graphene can be determined by: $\varepsilon_G = 1 + \frac{i\sigma_G\eta_0}{k_0 d}$, where d is thickness of graphene, η_0 and k_0 are the impedance and wave vector in air, respectively.

Appendix A. Supplementary data

Supplementary data associated with this article can be found, in the online version, at http://dx.doi.org/10.1016/j.apsusc.2017.07.051.

References

[1] S. Assefa, F.N. Xia, Y.A. Vlasov, Reinventing germanium avalanche photodetector for nanophotonic on-chip optical interconnects, Nature 464 (2010) 80–91.
[2] Z.F. Zhang, L.M. Wong, Z.W. Zhang, Z.Y. Wu, S.J. Wang, D.Z. Chi, R.D. Hong, W.F. Yang, Pulse laser deposition of epitaxial TiO_2 thin films for high-performance ultraviolet photodetectors, Appl. Surf. Sci. 355 (2015) 398–402.
[3] W. Deng, X.J. Zhang, L.M. Huang, X.Z. Xu, L. Wang, J.C. Wang, Q.X. Shang, S.T. Lee, J.S. Jie, Aligned single-crystalline perovskite microwire arrays for high-performance flexible image sensors with long-term stability, Adv. Mater 28 (2016) 2201–2208.
[4] X.J. Zhang, J.S. Jie, W. Deng, Q.X. Shang, J.C. Wang, H. Wang, X.F. Chen, X.H. Zhang, Adv. Mater 28 (2016) 2475–2503.
[5] L.B. Luo, F.X. Liang, J.S. Jie, Sn-catalyzed synthesis of SnO_2 nanowires and their optoelectronic characteristics, Nanotechnology 22 (2011) 485701.
[6] Y.G. Han, G. Wu, M. Wang, H.Z. Chen, Hybrid ultraviolet photodetectors with high photosensitivity based on TiO_2 nanorods array and polyfluorene, Appl. Surf. Sci. 256 (2009) 1530–1533.
[7] B. Nie, L.B. Luo, J.J. Chen, J.G. Hu, C.Y. Wu, L. Wang, Y.Q. Yu, Z.F. Zhu, J.S. Jie, Fabrication of p-type ZnSe:Sb nanowires for high-performance ultraviolet light photodetector application, Nanotechnology 24 (2013) 095603.
[8] T. Ji, Q. Liu, R.J. Zou, Y.G. Sun, K.B. Xu, L.W. Sang, M.Y. Liao, Y. Koide, L. Yu, J.Q. Hu, An interface engineered multicolor photodetector based on n-Si(111)/TiO_2 nanorod array hetero-junction, Adv. Funct. Mater. 26 (2016) 1400–1410.
[9] X.B. Chen, S.S. Mao, Titanium dioxide nanomaterials: synthesis, properties, modifications, and applications, Chem. Rev. 107 (2007) 2891–2958.
[10] D.Y. Zhang, C.W. Ge, J.Z. Wang, T.F. Zhang, Y.C. Wu, F.X. Liang, Single-layer graphene-TiO_2 nanotubes array heterojunction for ultraviolet photodetector application, Appl. Surf. Sci. 387 (2016) 1162–1168.
[11] Z.R. Wang, H. Wang, B. Liu, W.Z. Qiu, J. Zhang, S.H. Ran, H.T. Huang, J. Xu, H.W. Han, D. Chen, G.Z. Shen, Transferable and flexible nanorod-assembled TiO_2 cloths for dye-sensitized solar cells, photodetectors, and photocatalysts, ACS Nano 5 (2011) 8412–8419.

[12] M.J. Yang, J.L. Zhu, W. Liu, J.L. Sun, Novel photodetectors based on double-walled carbon nanotube film/TiO_2 nanotube array heterodimensional contacts, Nano Res. 4 (2011) 901–907.
[13] Z.R. Wang, S.H. Ran, B. Liu, D. Chen, G.Z. Shen, Multilayer TiO_2 nanorod cloth/nanorod array electrode for dye-sensitized solar cells and self-powered UV detectors, Nanoscale 4 (2012) 3350–3358.
[14] H.L. Xue, X.Z. Kong, Z.R. Liu, C.X. Liu, J.G. Zhou, W.Y. Chen, S.P. Ruan, Q. Xu, TiO_2 based metal-semiconductor-metal ultraviolet photodetectors, Appl. Phys. Lett. 90 (2007) 201118.
[15] X.Z. Kong, C.X. Liu, W. Dong, X.D. Zhang, C. Tao, L. Shen, J.R. Zhou, Y.F. Fei, S.P. Ruan, Metal-semiconductor-metal TiO_2 ultraviolet detectors with Ni electrodes, Appl. Phys. Lett. 94 (2009) 123502.
[16] H.S. Kim, J.W. Lee, N. Yantara, P.P. Boix, S.A. Kulkarni, S. Mhaisalkar, M. Gratzel, N.G. Park, High efficiency solid-state sensitized solar cell-based on submicrometer rutile TiO_2 nanorod and $CH_3NH_3PbI_3$ perovskite sensitizer, Nano Lett. 13 (2013) 2412–2417.
[17] M. Peng, Y. Liu, A. Yu, Y. Zhang, C. Liu, J. Liu, W. Wu, K. Zhang, X. Shi, J. Kou, J. Zhai, Z.L. Wang, Flexible self-powered GaN ultraviolet photoswitch with piezo-phototronic effect enhanced on/off ratio, ACS Nano 10 (2016) 1572–1579.
[18] P. Avouris, Graphene: electronic, photonic properties and devices, Nano Lett. 10 (2010) 4285–8294.
[19] X. Sheng, L.P. Chen, T. Xu, K. Zhu, X.J. Feng, Understanding and removing surface states limiting charge transport in TiO_2 nanowire arrays for enhanced optoelectronic device performance, Chem. Sci. 7 (2016) 1910–1913.
[20] Y.R. Xie, L. Wei, G.D. Wei, Q.H. Li, D. Wang, Y.X. Chen, S.S. Yan, G.L. Liu, L.M. Mei, J. Jiao, A self-powered UV photodetector based on TiO_2 nanorod arrays, Nanoscale Res. Lett 8 (2013) 188.
[21] L.H. Zeng, M.Z. Wang, H. Hu, B. Nie, Y.Q. Yu, C.Y. Wu, L. Wang, J.G. Hu, C. Xie, F.X. Liang, L.B. Luo, Monolayer graphene/germanium schottky junction as high-performance self-driven infrared light photodetector, ACS Appl. Mater. Interfaces 5 (2013) 9362–9366.
[22] T. Liang, G.Y. He, G.W. Huang, Y.H. Kong, W.F. Fu, W.F. Fu, H.Z. Chen, Q. Wang, H.D. Chen, D. Fujita, Y.C. Liu, M.S. Xu, Graphene nucleation preferentially at oxygen-rich Cu sites rather than on pure Cu surface, Adv. Mater. 27 (2015) 6404.
[23] M.S. Xu, D. Fujita, K. Sagisaka, E. Watanabe, N. Hanagata, Production of extended single-layer graphene, ACS Nano 5 (2011) 1522–1528.
[24] W.Y. Kong, G.A. Wu, K.Y. Wang, T.F. Zhang, Y.F. Zou, D.D. Wang, L.B. Luo, Graphene-beta-Ga_2O_3 heterojunction for highly sensitive deep UV photodetector application, Adv. Mater. 28 (2016) 10725–10731.
[25] B. Liu, E.S. Aydil, Growth of oriented single-crystalline rutile TiO_2 nanorods on transparent conducting substrates for dye-sensitized solar cells, J. Am. Chem. Soc. 131 (2009) 3985–3990.
[26] Y.M. Wang, K. Ding, B.Q. Sun, S.T. Lee, J.S. Jie, Two-dimensional layered material/silicon heterojunctions for energy and optoelectronic applications, Nano Res. 9 (2016) 72–93.
[27] M.S. Xu, T. Liang, M.M. Shi, H.Z. Chen, Graphene-like two-dimensional materials, Chem. Rev. 113 (2013) 3766–3798.
[28] C. Soci, A. Zhang, B. Xiang, S.A. Dayes, D.P.R. Aplin, J. Park, X.Y. Bao, Y.H. Lo, D. Wang, ZnO nanowire UV photodetectors with high internal gain, Nano Lett. 7 (2007) 1003–1008.
[29] J.G. Ok, J.Y. Lee, H.W. Baac, S.H. Tawfick, L.J. Guo, A.J. Hart, Rapid anisotropic photoconductive response of ZnO-coated aligned carbon nanotube sheets, Acs. Appl. Mater. Inter. 6 (2014) 874–881.
[30] B. Nie, J.G. Hu, L.B. Luo, C. Xie, L.H. Zeng, P. Lv, F.Z. Li, J.S. Jie, M. Feng, C.Y. Wu, Y.Q. Yu, S.H. Yu, Monolayer graphene film on ZnO nanorod array for high-performance schottky junction ultraviolet photodetectors, Small 9 (2013) 2872–2879.
[31] E. Enache-Pommer, B. Liu, E.S. Aydil, Electron transport and recombination in dye-sensitized solar cells made from single-crystal rutile TiO_2 nanowires, Phys. Chem. Chem. Phys. 11 (2009) 9648–9652.
[32] S. Wendt, P.T. Sprunger, E. Lira, G.K.H. Madsen, Z.S. Li, J.O. Hansen, J. Matthiesen, A. Blekinge-Rasmussen, E. Laegsgaard, B. Hammer, F. Besenbacher, The role of interstitial sites in the Ti3d defect state in the band gap of titania, Science 320 (2008) 1755–1759.
[33] B. Santara, P.K. Giri, K. Imakita, M. Fujii, Evidence of oxygen vacancy induced room temperature ferromagnetism in solvothermally synthesized undoped TiO_2 nanoribbons, Nanoscale 5 (2013) 5476–5488.
[34] B. Santara, P.K. Giri, K. Imakita, M. Fujii, Evidence for Ti interstitial induced extended visible absorption and near infrared photoluminescence from undoped TiO_2 nanoribbons: an in situ photoluminescence study, J. Phys. Chem. C 117 (2013) 23402–23411.
[35] X.H. Lu, G.M. Wang, T. Zhai, M.H. Yu, J.Y. Gan, Y.X. Tong, Y. Li, Hydrogenated TiO_2 nanotube arrays for supercapacitors, Nano Lett. 12 (2012) 1690–1696.
[36] Q. Kang, J.Y. Cao, Y.J. Zhang, L.Q. Liu, H. Xu, J.H. Ye, Reduced TiO_2 nanotube arrays for photoelectrochemical water splitting, J. Mater. Chem. A 1 (2013) 5766–5774.
[37] Z. Liang, G.Y. Zheng, W.Y. Li, Z.W. Seh, H.B. Yao, K. Yan, D.S. Kong, Y. Cui, Sulfur cathodes with hydrogen reduced titanium dioxide inverse opal structure, Acs Nano 8 (2014) 5249–5256.
[38] R. Lu, C.W. Ge, Y.F. Zou, K. Zheng, D.D. Wang, T.F. Zhang, L.B. Luo, A localized surface plasmon resonance and light confinement-enhanced near-infrared light photodetector, Laser Photonics Rev. 10 (2016) 595–602.
[39] B.D. Boruah, D.B. Ferry, A. Mukherjee, A. Misra, Few-layer graphene/ZnO nanowires based high performance UV photodetector, Nanotechnology 26 (2015) 235703.
[40] K. Zheng, L.B. Luo, T.F. Zhang, Y.H. Liu, Y.Q. Yu, R. Lu, H.L. Qiu, Z.J. Li, J.C.A. Huang, Optoelectronic characteristics of a near infrared light photodetector based on a topological insulator Sb_2Te_3 film, J. Mater. Chem. C 3 (2015) 9154–9160.
[41] J.S. Jie, W.J. Zhang, Y. Jiang, X.M. Meng, Y.Q. Li, S.T. Lee, Photoconductive characteristics of single-crystal CdS nanoribbons, Nano Lett. 6 (2006) 1887–1892.
[42] L.B. Luo, Y.F. Zou, C.W. Ge, K. Zheng, D.D. Wang, R. Lu, T.F. Zhang, Y.Q. Yu, Z.Y. Guo, A surface plasmon enhanced near-infrared nanophotodetector, Adv. Opt. Mater. 4 (2016) 763–771.